Flexible CoAl LDH@PEDOT Core/Shell Nanoplatelet Array for High-Performance Energy Storage

Jingbin Han, Yibo Dou, Jingwen Zhao, Min Wei, David G. Evans, and Xue Duan*

***A** CoAl-layered double hydroxide (LDH)@poly(3,4-ethylenedioxythiophene) (PEDOT) core/shell nanoplatelet array (NPA) is grown on a flexible Ni foil substrate as a high-performance pseudocapacitor. The LDH@PEDOT core/shell NPA shows a maximum specific capacitance of 649 F/g (based on the total mass) by cyclic voltammetry (scan rate: 2 mV/s) and 672 F/g by galvanostatic discharge (current density: 1 A/g). Furthermore, the hybrid NPA electrode also exhibits excellent rate capability with a specific energy of 39.4 Wh/kg at a current density of 40 A/g, as well as good long-term cycling stability (92.5% of its original capacitance is retained after 5000 cycles). These performances are superior to those of conventional supercapacitors and LDH NPA without the PEDOT coating. The largely enhanced pseudocapacitor behavior of the LDH@PEDOT NPA electrode is related to the synergistic effect of its individual components: the LDH nanoplatelet core provides abundant energy-storage capacity, while the highly conductive PEDOT shell and porous architecture facilitate the electron/mass transport in the redox reaction.*

1. Introduction

The depletion of traditional energy resources as well as global warming evoke considerable attention in developing advanced energy-storage and delivery systems. Electrochemical capacitors (also known as supercapacitors or ultracapacitors), as emerging energy storage devices, have attracted intensive interest due to their high power density, long cycle life, short charging time and good safety record.[1–7] Pseudocapacitors (or redox capacitors)[8–12] represent one type of supercapacitors that have the potential to achieve high specific energy resulting from the fast and reversible redox reactions of the active material. Among various pseudocapacitor materials, hydrous RuO_2 exhibits the highest performance to date,[13–15] but the scarcity in nature and high cost limit its commercial application. Therefore, much effort has been devoted in exploring alternative electrode materials possessing pseudocapacitive behavior, such as manganese oxide,[16–20] cobalt oxide/hydroxide,[21–23] nickel oxide/hydroxide[25–27] and molybdenum oxide.[28,29]

In spite of high energy density of pseudocapacitive materials, two serious problems remain not well resolved in their practical applications. Firstly, the aggregation of active materials tends to reduce the accessible surface area for participating electrochemical reaction, which in turn decreases the specific capacitance. Secondly, the low conductivity of pseudocapacitive materials restricts the electron-transfer rate, resulting in inferior performance at high charge-discharge current density. Therefore, the rational design of novel electrode based on structural and compositional considerations is highly essential for achieving high-performance supercapacitors.[30–33] One effective approach is to anchor electroactive materials on specific substrate to fabricate ordered array electrode as well as to improve the conductivity *via* incorporation of highly conductive polymers.[34] The resulting new type of electrode would possess the following advantages: (i) the well-arrayed electroactive material provides large

---

Dr. J. Han, Y. Dou, J. Zhao, Prof. M. Wei,
Prof. D. G. Evans, Prof. X. Duan
State Key Laboratory of
Chemical Resource Engineering
Beijing University of Chemical Technology
Box 98, Beijing 100029, PR China
Fax: (+86)10-6442-5385
E-mail: weimin@mail.buct.edu.cn

DOI: 10.1002/smll.201201336

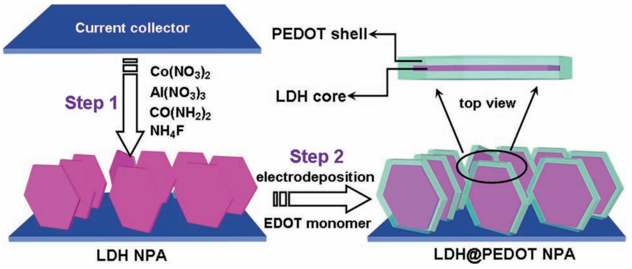

Scheme 1. Schematic illustration for the fabrication of LDH@PEDOT core/shell nanoplatelet array electrode.

specific surface area for the redox reaction as well as effective pathway for fast electron transport between electroactive center and current collector; (ii) the enhanced conductivity of the electrode reduces the interfacial resistance, which consequently accelerates electron transfer at high charge-discharge current density; (iii) the feasible design strategy guarantees facile manipulation and long-term stability of energy storage devices.

Layered double hydroxides (LDHs), also known as anionic clays,[35–39] are promising pseudocapacitive materials owing to their high redox activity,[40,41] low cost and environmentally friendly nature. Herein, we demonstrate the design and fabrication of CoAl–LDH@poly(3,4-ethylenedioxythiophene) (PEDOT) core/shell nanoplatelet array (NPA) grown on flexible Ni foil substrate for high-performance pseudocapacitor. The maximum specific capacitance of 649 F/g (based on the total mass) by cyclic voltammetry (scan rate: 2 mV/s) and 672 F/g by galvanostatic discharge (current density: 1 A/g) were achieved. The hybrid LDH@PEDOT NPA electrode also exhibits excellent rate capability with a specific energy of 39.4 Wh/kg at a current density of 40 A/g, as well as good long-term cycling stability (only 7.5% loss of initial capacitance after 5000 cycles). The specific capacitance of the LDH@PEDOT NPA electrode is comparable with RuO_2 and superior to MnO_2, NiO and MoO_3-base supercapacitors,[9,13,18] although the specific energy is not the highest.[25] The synergistic effect of individual components was studied in detail, which plays a key role in determining the high-performance of the LDH@PEDOT NPA electrode. Therefore, this work provides a promising approach for the design and fabrication of novel core/shell structure with largely enhanced supercapacitive behavior, which can be potentially applied in energy storage/conversion devices.

2. Results and Discussion

Our approach for fabricating hybrid LDH@PEDOT core/shell NPA as pseudocapacitive electrode involves two key steps, as shown in **Scheme 1**. Firstly, vertically aligned CoAl–LDH NPA on Ni foil substrate was prepared *via* a facile hydrothermal method (see details in the Supporting Information, Scheme S1 and Figure S1). Subsequently, a thin layer of conductive polymer PEDOT was coated onto the surface of as-prepared LDH NPA by electrodeposition technique. **Figure 1**a illustrates the X-ray diffraction (XRD) patterns of the LDH film on Ni foil and the corresponding powder sample scraped from the film for comparison. The powder material shows a series of reflections at 11.7°, 23.5°, 34.8°, 39.2°, 46.8°, 59.7° and 60.9°, corresponding to the [003], [006], [012], [015], [018], [110] and [113] reflections of an randomly stacked CO_3^{2-}-LDH phase, respectively.[42] For the LDH film on Ni substrate, the absence of [00*l*] reflections indicates a preferential orientation of LDH crystallites with their *ab* plane perpendicular to the substrate. The optical image (Figure 1b) of the CoAl–LDH film reveals good flexibility and excellent mechanical robustness of the LDH NPA upon repeated bending.

Figure 1c and 1d display top-view scanning electron microscopy (SEM) observations of the LDH NPA, from which uniform hexagonal plate-like microcrystals were observed with diameter of 4–5 μm and thickness of ~40 nm. The LDH film has an open-up network structure composed by interconnected nanoplatelet building blocks, whose structure formation is governed by a "heterogeneous nucleation growth" mechanism.[43] A representative cross-sectional SEM image (Figure 1e) shows that the LDH NPA with an average lateral size of ~5 μm is approximately vertically aligned on the supporting substrate, in consistent with the XRD results (Figure 1a). The typical transmission electron microscopy (TEM) observation (Figure 1f) reveals the hexagonal morphology of a single LDH microcrystal, which displays a lattice spacing of 0.26 nm (Figure 1g) ascribed to the [012] crystal plane of LDH material. The corresponding selected-area electron diffraction (SAED) pattern (Figure 1h) exhibits hexagonally arranged bright spots, indicating its single-crystal nature.

An ideal supercapacitive material should have excellent electrical conductivity to support fast electron transport, especially at high charge-discharge rate. In order to improve the conductivity of the as-grown LDH NPA, a thin layer of conductive polymer, poly(3,4-ethylenedioxythiophene) (PEDOT) was coated onto the surface of LDH NPA *via* potentiostatic electrodeposition method to fabricate LDH@PEDOT core/shell architecture. The optimum voltage was determined as 1.0 V vs Ag/AgCl electrode according to the cyclic voltammograms (CV) curve of EDOT monomer (see details in the Supporting Information, Figure S2–S4). The SEM (**Figure 2**a–f) and TEM (Supporting Information, Figure S5) images clearly demonstrate the core/shell nanostructure, whose shell thickness increases along with elongation of deposition time. Herein, the mass of the PEDOT shell can be well controlled by changing the deposition time, as shown in Figure S6 (see the Supporting Information). Energy dispersive X–ray spectra (EDS) (Figure 2g, Figure S7) show a gradual signal increase of sulfur element, demonstrating the deposition of PEDOT shell on LDH core. Moreover, the Raman spectrum (Figure 2h) further confirms the formation of LDH@PEDOT hybrid material, which displays both absorption peak at 1054 cm^{-1} originating from LDH and two signals at 1340 and 1590 cm^{-1} attributed to PEDOT.[44] The pores or voids between nanoplatelets will act as effective transportation channels for the electrolyte during charge-discharge process. N_2 gas adsorption-desorption measurement on LDH@PEDOT NPA (Figure 2i) reveals that the

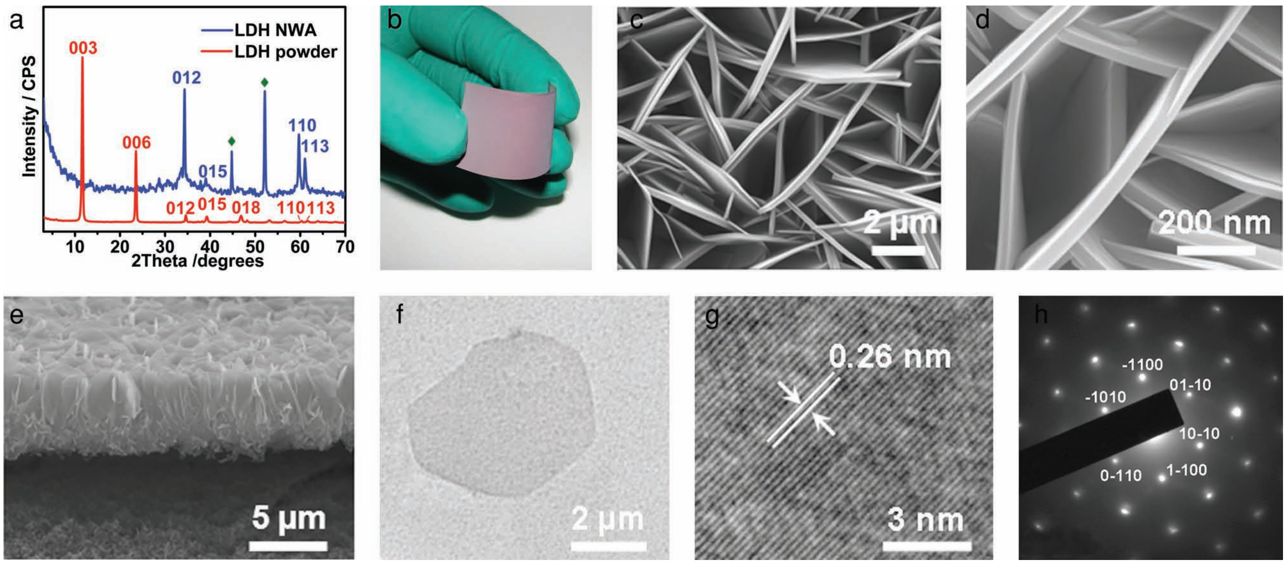

Figure 1. a) XRD patterns of as-prepared LDH NPA on Ni foil substrate and the corresponding powder sample scraped from the substrate; two reflections denoted with rhombus originate from the substrate. b) Optical, c,d) top-view SEM images and e) cross-sectional SEM image of large-scale CoAl–LDH NPA on Ni foil substrate. f) TEM and g) high-resolution TEM image of an individual CoAl–LDH nanoplatelet and h) the corresponding SAED pattern.

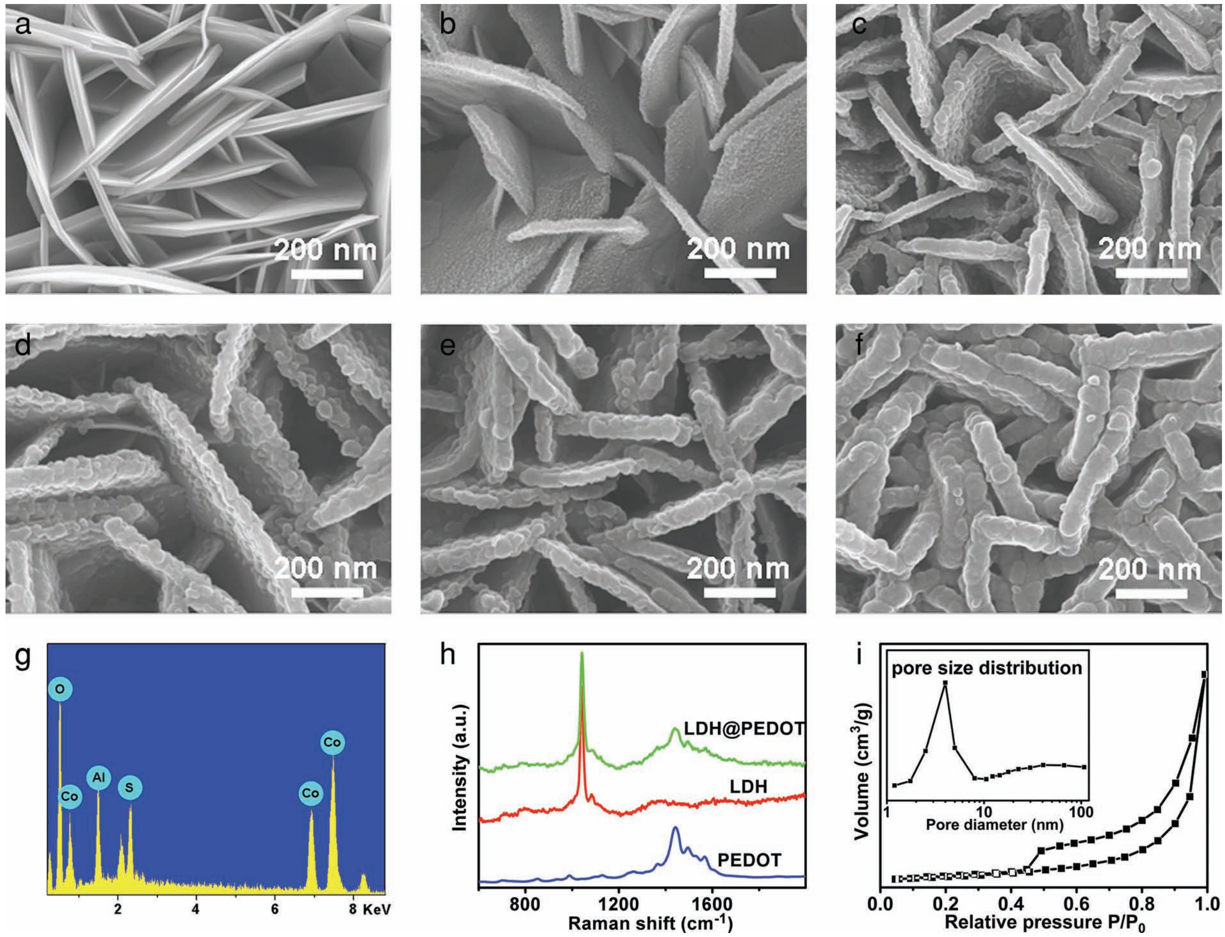

Figure 2. a–f) SEM images of the LDH@PEDOT NPA obtained by electrodeposition for various times: $t = 90$ s, 120 s, 150 s, 180 s, 210 s, and 240 s for (a–f), respectively. g) A representative EDS spectrum of the LDH@PEDOT NPA shown in (e). h) Raman spectra of the LDH NPA, PEDOT, and LDH@PEDOT NPA. i) Nitrogen adsorption–desorption isotherms and corresponding pore size distribution (inset) of the LDH@PEDOT NPA with an electrodeposition time of 210 s.

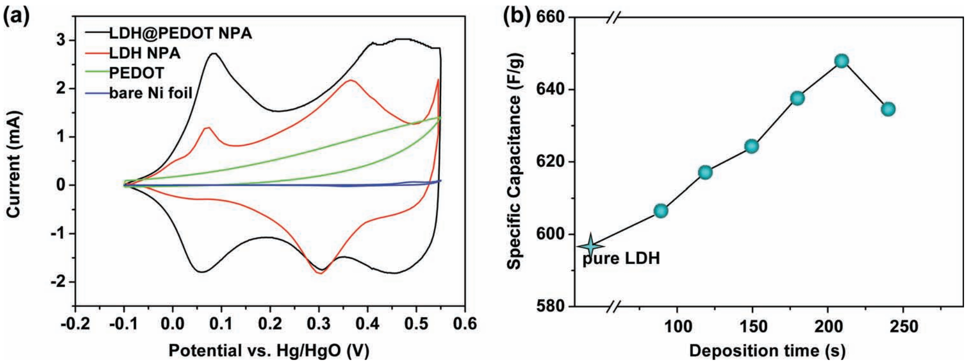

Figure 3. (a) CV curves of the LDH NPA, PEDOT, LDH@PEDOT NPA and bare Ni foil electrode measured at a scan rate of 2 mV/s; note that the signal from Ni foil is negligible and PEDOT shows no redox reaction in the applied potential window; (b) The C_{sp} value (obtained from CV curves) of the LDH@PEDOT NPA electrode as a function of deposition time.

sample displays type IV isotherms with H3 type hysteresis loops, with a mesopore distribution in the size 2–6 nm. It has been reported that a mesoporous structure is favorable for the supercapacitive behavior,[45] which will be discussed in the next section.

Cyclic voltammetry (CV) was carried out to study the electrochemical capacitive performance of the pristine LDH and LDH@PEDOT NPA electrode using a three-electrode system. For the LDH NPA electrode, two pairs of anodic/cathodic peaks (~0.03 and ~0.32 V) superimposed on a broad redox background are observed (**Figure 3**a), which can be attributed to the following Faradaic reaction of Co(II)/Co(III) (Equation 1) and Co(III)/Co(IV) (Equation 2), respectively (for simplicity, CoAl–LDH is denoted as LDH–Co(OH)$_2$, since Al is an electrochemically inert element).[46]

$$\text{LDH–Co(OH)}_2 + \text{OH}^- \Longleftrightarrow \text{LDH–CoOOH} + \text{H}_2\text{O} + e^- \qquad (1)$$

$$\text{LDH–CoOOH} + \text{OH}^- \Longleftrightarrow \text{LDH–CoO}_2 + \text{H}_2\text{O} + e^- \qquad (2)$$

The specific capacitance (C_{sp}) of bare LDH NPA was calculated to be 578 F/g based on CV curve at a scan rate of 2 mV/s. After electrodeposition of PEDOT wrap, the CV profile changed markedly to quasi-rectangular shape, especially in the lower potential range, which indicates a significant increase of the capacitance. With elongating deposition time, the specific capacitance of LDH@PEDOT core/shell NPA (obtained from CV measurement) increased at first to a maximum (649 F/g) with PEDOT: LDH weight ratio of 0.233: 1 (t = 210 s) and then decreased upon further deposition (Figure 3b). Therefore, the LDH@PEDOT NPA with t = 210 s was chosen as the optimum electrode for further evaluation of electrochemical performance. **Figure 4**a,c show CV curves of the pristine LDH NPA and LDH@PEDOT NPA electrodes at various scan rates. The specific capacitance of LDH NPA changes from 578 F/g to 207 F/g as scan rate increasing from 2 mV/s to 40 mV/s (Figure 4b). While the specific capacitance of the LDH@PEDOT NPA was calculated (based on total sample mass) to be 649, 597, 560, 544, 501 and 445 F/g at the scan rate of 2, 5, 10, 20, 30 and 40 mV/s, respectively (Figure 4d). The results indicate that the LDH@PEDOT NPA composite shows largely enhanced electrochemical performance compared with the pristine LDH NPA electrode, which is ascribed to the increased utilization ratio of the electroactive species originating from the improved conductivity by the incorporation of PEDOT shell.

Rate capability is one of the important factors in evaluating the power application of supercapacitors. The constant-current galvanostatic (GV) charge-discharge curves of the pristine LDH and LDH@PEDOT NPA electrode at different current density were measured. The pristine LDH NPA electrode shows a specific capacitance of ~584 F/g at a current density of 1 A/g and ~172 F/g at 40 A/g (**Figure 5**a,b), with a loss of 71% at 40 A/g. In comparison, the LDH@PEDOT NPA electrode exhibits a specific capacitance of ~672 F/g at 1 A/g, which is still as high as ~424 F/g even at a high current density of 40 A/g (Figure 5c,d), demonstrating its superior high-rate capability. The enhanced capacitance and high-rate capability of the LDH@PEDOT NPA is attributed to the improvement of electrical conductivity of the electrode after coating with PEDOT, which will be further discussed in the next section.

To demonstrate the advantages of the LDH@PEDOT NPA electrode originating from its oriented array feature, galvanostatic tests were also performed on counterpart samples obtained by scratching the LDH and LDH@PEDOT NPA respectively from the substrate and subsequently by pressing a mixture of the scratched sample and polytetrafluoroethylene (PTFE) binder onto a nickel foam current collector. For powder samples of LDH and LDH@PEDOT–Ni foam electrode, although both of them exhibit nearly 100% coulombic efficiency with good electrochemical reversibility, the values of specific capacitance at a current density of 1 A/g (**Figure 6**) are much lower (286 and 334 F/g for LDH–Ni foam and LDH@PEDOT–Ni foam electrode, respectively) than their well-arranged counterpart (584 and 672 F/g for LDH NPA and LDH@PEDOT NPA electrode, respectively). The results indicate that the specific array material with mesoporous and well-ordered structure enhances ion diffusion of the electrolyte and electron transfer between the aligned NPA and the underneath substrate.

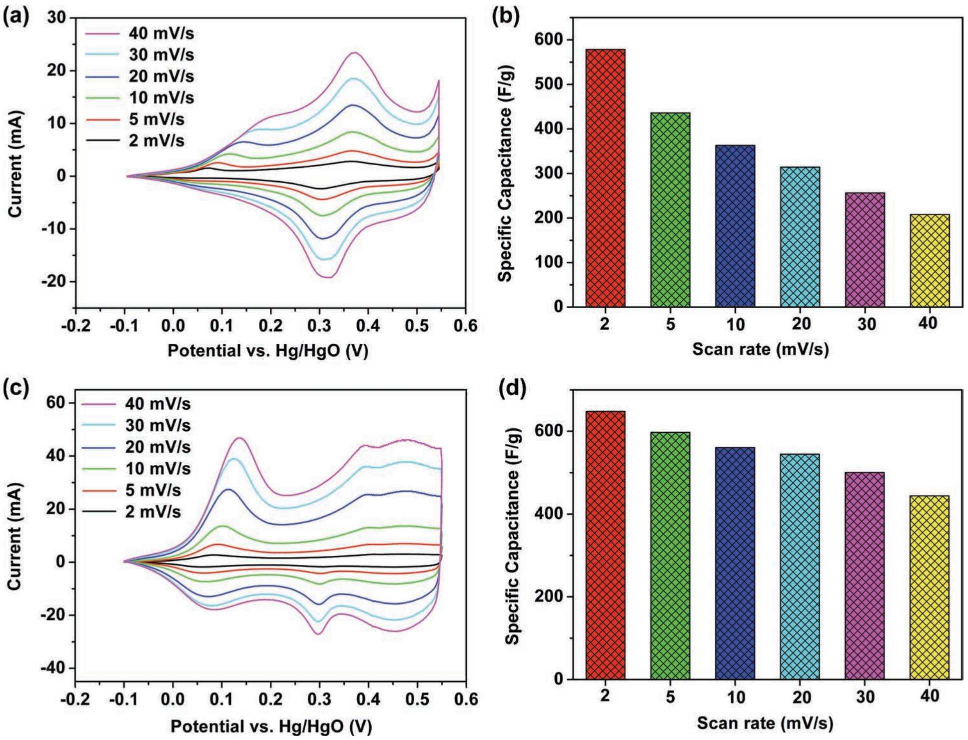

Figure 4. CV curves and specific capacitance of the (a,b) pristine LDH NPA and (c,d) LDH@PEDOT NPA electrodes at various scan rates.

The fast ion diffusion and effective electron transfer in the well-ordered LDH@PEDOT NPA electrode were further confirmed by the electrochemical impedance spectroscopy (EIS) (**Figure 7**a). The Nyquist diagrams of all the four electrodes (LDH NPA, LDH@PEDOT NPA, LDH–Ni foam, LDH@PEDOT–Ni foam) exhibit a semicircle over the high frequency range, followed by a linear part in the low frequency region. The linear part corresponds to the

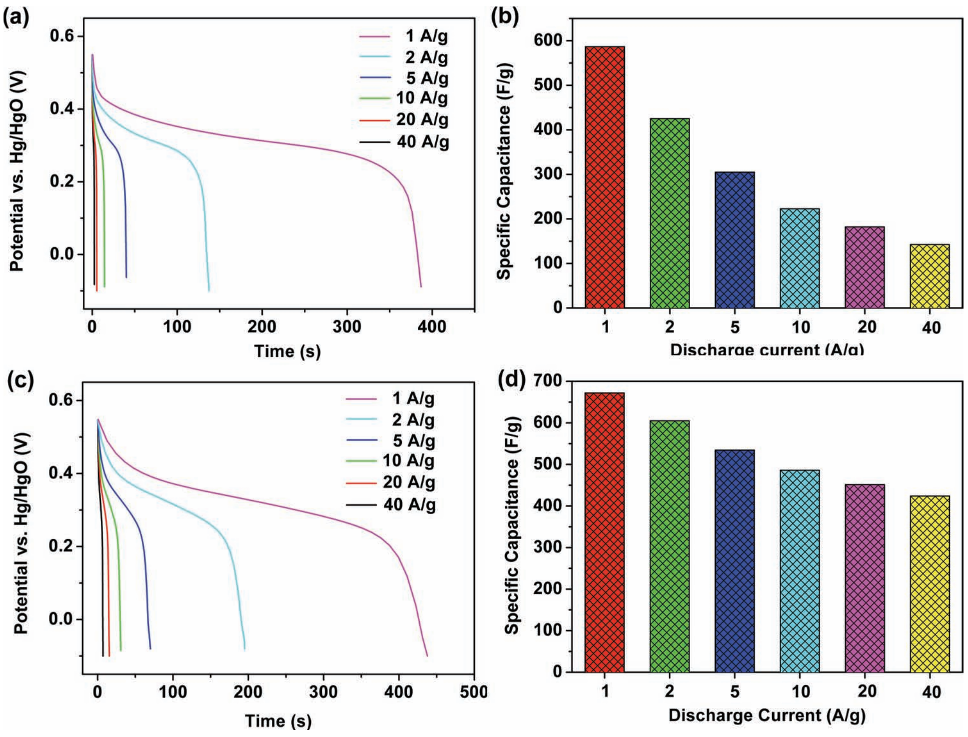

Figure 5. Galvanostatic discharge curves and specific capacitance of the (a,b) pristine LDH NPA and (c,d) LDH@PEDOT NPA electrode at various discharge current density.

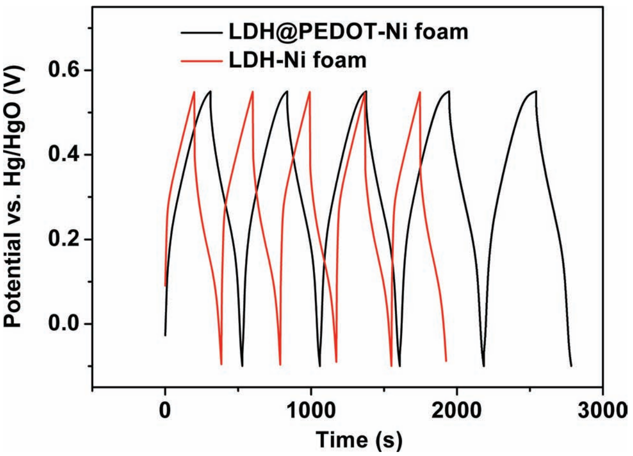

Figure 6. Galvanostatic charge-discharge curves of the LDH–Ni foam and LDH@PEDOT–Ni foam electrodes at a current density of 1 A/g.

Warburg impedance (W), which is described as a diffusive resistance[47] of the OH^- ion within the electrode pores. The slope of the straight line at low frequency for the LDH@PEDOT NPA is comparable with that of LDH NPA; both of them are larger than that of the LDH@PEDOT–Ni foam and LDH–Ni foam. This indicates that the electrolyte diffusion resistance for the well-aligned electrode is much lower than that of the randomly stacked electrode, which is consistent with the superior pseudocapacitor performance of the arrayed electrode. The impedance at high frequency (100 kHz) reflects the equivalent series resistance (ESR) in the electrode/electrolyte system, which is related to the electrical conductivity of the electrode.[48] The ESR of LDH@PEDOT NPA, LDH NPA, LDH@PEDOT–Ni foam and LDH–Ni foam is 1.9, 3.3, 2.9 and 3.8 Ω, respectively, demonstrating the highest conductivity of the LDH@PEDOT NPA electrode. In addition, the semicircle of the Nyquist diagram corresponds to the Faradaic reactions and its diameter represents the interfacial charge-transfer resistance (usually termed Faradaic resistance).[49] The charge-transfer resistance R_{ct} of the LDH@PEDOT NPA is the smallest one among these four electrodes. The lower charge-transfer resistance for the LDH@PEDOT NPA electrode compared with pristine LDH NPA was further confirmed by the larger exchange current density (i^0), as revealed by Tafel curve (see Supporting Information, Figure S8). The results above demonstrate that the combination of fast ion diffusion, high electrical conductivity as well as low electron-transfer resistance is responsible for the excellent electrochemical performance of the LDH@PEDOT NPA electrode.

Specific energy and specific power are two key factors for practical applications of electrochemical supercapacitors. A good electrochemical supercapacitor is expected to provide high specific energy or high specific capacitance in rapid charging-discharging process (current density). Figure 7b shows the specific energy *vs*. specific power plot of the four electrodes (LDH NPA, LDH@PEDOT NPA, LDH–Ni

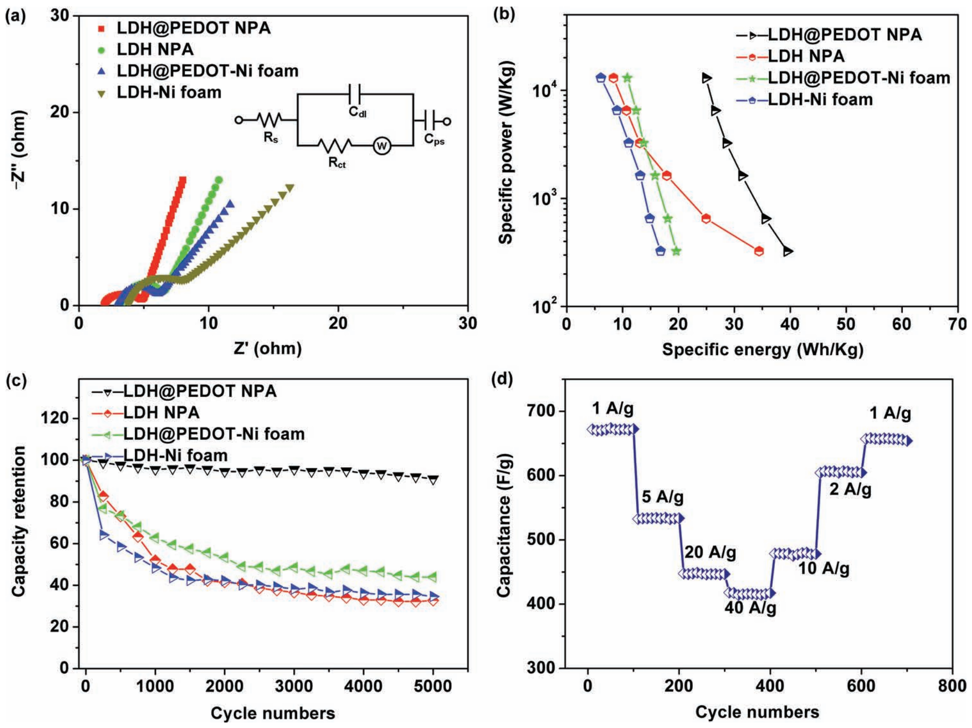

Figure 7. (a) Nyquist plots of the electrochemical impedance spectroscopy (EIS) performed between 0.01 and 100 kHz (the inset shows the equivalent circuit diagram of different elements, where R_s, R_{ct}, C_{dl}, C_{ps} and W represent the electrolyte resistance, charge-transfer resistance, double layer capacitance, pseudocapacitance and interfacial diffusive resistance, respectively); (b) specific energy *vs*. specific power plot and (c) cycling stability of the LDH NPA, LDH@PEDOT NPA, LDH–Ni foam and LDH@PEDOT–Ni foam electrode, respectively; (d) cycling stability of the LDH@PEDOT NPA at consecutively varied current density.

foam, LDH@PEDOT–Ni foam) as the GV charge-discharge current increased from 1 to 40 A/g. The specific energy for LDH–Ni foam, LDH@PEDOT–Ni foam and LDH NPA electrode are 16.8, 19.6 and 34.4 Wh/kg at 40 A/g. In contrast, the LDH@PEDOT NPA electrode displays largely enhanced specific energy. Remarkably high specific energy and specific power values of 39.4 Wh/kg (40 A/g) and 13 kW/kg (1 A/g) were obtained, respectively. These values are much superior to those of conventional supercapacitors, demonstrating the capability of LDH@PEDOT NPA as energy supply component in large-power electrical appliances.

Cycling capability or cycling life is another important requirement for supercapacitor applications. The cycling life tests for LDH NPA, LDH@PEDOT NPA, LDH–Ni foam, LDH@PEDOT–Ni foam electrode were carried out at a current density of 10 A/g using galvanostatic charge-discharge technique. As shown in Figure 7c, the LDH NPA, LDH–Ni foam and LDH@PEDOT–Ni foam electrode lose 68%, 52% and 57% of their original capacitance respectively over 5000 cycles. In the case of the LDH@PEDOT NPA electrode however, 92.5% of its original capacitance is retained after 5000 cycles, and the charge-discharge curves for the last 10 cycles remain unchanged compared with the first 10 cycles (Supporting Information, Figure S9), illustrating its excellent long-term cyclability. The better cycling stability of LDH@PEDOT NPA compared with LDH@PEDOT-Ni foam electrode further testifies the advantage of NPA architecture for electrochemical energy storage, as a result of its ordered stacking as well as strong anchoring to the substrate. For the LDH@PEDOT-Ni foam electrode however, the randomly stacked LDH powdered material and poor adhesion to the substrate may induce high ion-diffusion resistance and structural collapse in long-term charge-discharge cycling. Furthermore, the bending LDH@PEDOT NPA electrode exhibits almost the same C_{sp} value to unbent sample, as well as excellent cycling stability (see the Supporting Information, Figure S10), indicating its capability as a flexible energy storage device. Figure 7d further reveals the current density dependence of the cycling performance, from which a stable capacitance at consecutively varied current density of the LDH@PEDOT NPA electrode was observed. Inspiringly, the LDH/PEDOT NPA electrode shows robust mechanical stability. After long-term cycling, the original structure of the LDH@PEDOT NPA is preserved without obvious deformation; while the pristine LDH NPA electrode undergoes serious collapse (see the Supporting Information, Figure S11). From this perspective, the presence of PEDOT greatly enhances the structural stability of the LDH@PEDOT NPA electrode during the redox reaction.

3. Conclusion

In summary, a facile and cost-effective approach is developed to fabricate high-performance flexible supercapacitors based on a LDH@PEDOT core/shell NPA electrode. The LDH nanoplatelet core provides high energy-storage capacity through a fast and reversible redox reaction, while the highly conductive PEDOT shell facilitates electron transport during the charge–discharge process. The LDH/PEDOT NPA electrode exhibits excellent electrochemical behavior, including a high specific capacitance, a good rate capability, remarkable cycling performance, and a high specific energy and power. This greatly enhanced performance can be attributed to the high level of orientation, good conductivity, and suitable mesopore distribution of the active materials, which improve the faradaic redox reaction and benefit the mass transport of electrolytes. The design strategy for highly oriented array electrodes presented here can be generalized to the fabrication of other heterogeneous nanocomposite structures based on hydroxides/oxides and conductive polymers, for the purpose of obtaining high-performance supercapacitors.

4. Experimental Section

Synthesis of LDH Nanoplatelet Array on a Ni Foil Substrate: The LDH nanoplatelet array was synthesized by a homogeneous hydrothermal method. Typically, 15 mmol of $Co(NO_3)_2·6H_2O$, 5 mmol of $Al(NO_3)_3·9H_2O$, 20 mmol of NH_4F and 50 mmol of $CO(NH_2)_2$ were dissolved in 100 mL of water, and were transferred into a Teflon-lined stainless steel autoclave. A piece of clean Ni foil (size: 3 cm × 6 cm, thickness: ~60 μm) was then immersed into the solution. Subsequently, the autoclave was sealed and maintained at 110 °C for 8 h. After the reaction, LDH nanoplatelet aggregate and nanoplatelet array were observed on the upside and backside of substrate, respectively (see the Supporting Information, Scheme S1). In order to eliminate the influence of LDH aggregate deposited on the upside, this side was rinsed thoroughly to remove the surface material and then was coated with a thin layer of electrochemically inert and nonconductive poly(methyl methacrylate) (PMMA) by a cast-coating technique. Subsequently the substrate was dried at 100 °C for 5 min.

Synthesis of LDH@PEDOT Core/Shell Nanoplatelet Arrays: a thin coating of PEDOT was deposited onto the surface of LDH nanoplatelet array by potentiostatic electrodeposition technique in an aqueous medium (0.07 M SDS + 0.1 M $LiClO_4$ + 0.05 M EDOT). Voltammetric experiments were performed to determine the deposition potential of PEDOT in a three electrode electrochemical cell with glassy carbon, Pt wire and Ag/AgCl as the working, counter and reference electrode, respectively. The optimum voltage for the PEDOT film deposition is fixed at 1.0 V *vs* Ag/AgCl electrode according to the cyclic voltammograms curve (see the Supporting Information, Figure S2). Afterwards, the LDH NPA on Ni foil was used as the working electrode for the deposition of PEDOT wrap. The deposition time was varied from 90 to 240 s to control the thickness of the PEDOT shell. All solutions were deoxygenated by nitrogen before the electrochemical measurements.

Fabrication of LDH–Ni Foam and LDH@PEDOT–Ni Foam Electrodes: the pristine LDH NPA and LDH@PEDOT NPA were scratched from the substrate respectively to give a comparison study with their well-aligned array counterpart. The working electrode was prepared as follows: ~2 mg of the scratched material was first mixed with polytetrafluoroethylene (PTFE) with LDH (or LDH@PEDOT):PTFE ratio of 50:1 by weight and then was dispersed in ethanol; the suspension was drop-dried onto a Ni foam (~1.6 cm^2) at 80 °C overnight. The foam was pressed at ~5 MPa before measurement.

Material Characterization: products were characterized by powder X-ray diffraction (Shimadzu XRD-6000), scanning electron microscopy (Zeiss Supra 55) equipped with an energy dispersive X-ray spectrometer (EDS), transmission electron microscopy (JEOL JEM-2100), and Raman spectroscopy (Renishaw, inVia-Reflex, 633 nm). The weight ratio of LDH: PEDOT on Ni foil substrate was measured on an inductively coupled plasma spectroscopy (ICP) instrument (Shimadzu ICPS-7500). Pore size distribution plots were obtained by Barrett-Joyner-Halenda (BJH) method using a Micromeritics ACAP 2020 analyzer. Prior to the measurements, samples were degassed at 120 °C for 6 h. Cyclic voltammetry (CV) and galvanostatic (GV) charge–discharge measurements were performed on a CHI 660C electrochemistry workstation using a three-electrode mode in 6 M KOH aqueous solution within the potential window of –0.1 to 0.55 V. The LDH@PEDOT nanoplatelet array was directly used as the working electrode. The reference and counter electrode were Hg/HgO and a platinum wire, respectively. Electrochemical impedance spectra (EIS) measurements were performed by applying an AC voltage with 5 mV amplitude in a frequency range from 0.01 to 100 kHz, using the same setup as CV and GV tests. Tafel polarization tests were carried out at a linear scan rate of 1 mV/s.

Average specific capacitance values were calculated from the CV curves using the following equation:

$$C = \frac{1}{sm\,(V_H - V_L)} \int_{V_L}^{V_H} i\,dV \tag{3}$$

where *i* is the oxidation or reduction current; *s* is scanning rate; *m* indicates the mass of the active material; V_H and V_L represent high and low potential limit of the CV tests. Specific capacitance was also calculated from the galvanostatic charge-discharge curves, by the equation:

$$C = \frac{i\Delta t}{m\Delta V} \tag{4}$$

where *i* is the discharge current; Δ*t* is the discharge time; *m* indicates the mass of the active material, and Δ*V* corresponds to the voltage change after a full charge or discharge process. Specific energy (*E*) was derived from the galvanostatic discharge curves using the following equation:

$$E = \frac{1}{2} C \Delta V^2 \tag{5}$$

where *C* is the specific capacitance of the active material, and Δ*V* is the voltage range of one sweep segment. Specific power (*P*) was calculated based on the following equation:

$$P = \frac{E}{\Delta t} \tag{6}$$

where *E* is the specific energy; Δ*t* is the discharge time.

Supporting Information

Supporting Information is available from the Wiley Online Library or from the author.

Acknowledgements

This project was supported by the National Natural Science Foundation of China, the 973 Program (Grant No.: 2011CBA00504), the Collaboration Project from the Beijing Education Committee, and the Fundamental Research Funds for the Central Universities (Grant No.: ZY1215).

---

[1] P. Simon, Y. Gogotsi, *Nat. Mater.* **2008**, *7*, 845.
[2] L. Yuan, X. Lu, X. Xiao, T. Zhai, J. Dai, F. Zhang, B. Hu, X. Wang, L. Gong, J. Chen, C. Hu, Y. Tong, J. Zhou, Z. L. Wang, *ACS Nano* **2012**, *6*, 656.
[3] L. Dai, D. W. Chang, J.-B. Baek, W. Lu, *Small* **2012**, *8*, 1130.
[4] X. Lang, A. Hirata, T. Fujita, M. Chen, *Nat. Nanotechnol.* **2011**, *6*, 232.
[5] G. Wang, X. Sun, F. Lu, H. Sun, M. Yu, W. Jiang, C. Liu, J. Lian, *Small* **2012**, *8*, 452.
[6] J. Bae, M. K. Song, Y. J. Park, J. M. Kim, M. Liu, Z. L. Wang, *Angew. Chem. Int. Ed.* **2011**, *50*, 1683.
[7] Y. Zhu, S. Murali, M. D. Stoller, K. J. Ganes, W. Cai, P. J. Ferreira, A. Pirkle, R. M. Wallace, K. A. Cychosz, M. Thommes, D. Su, E. A. Stach, R. S. Ruoff, *Science* **2011**, *332*, 1537.
[8] Y.-B. He, G.-R. Li, Z.-L. Wang, C.-Y. Su, Y.-X. Tong, *Energy Environ. Sci.* **2011**, *4*, 1288.
[9] L.-Q. Mai, F. Yang, Y.-L. Zhao, X. Xu, L. Xu, Y.-Z. Luo, *Nat. Commun.* **2011**, *2*, 381.
[10] Z.-S. Wu, W. Ren, D.-W. Wang, F. Li, B. Liu, H.-M. Cheng, *ACS Nano* **2010**, *4*, 5835.
[11] G. Yu, L. Hu, M. Vosgueritchian, H. Wang, X. Xie, J. R. McDonough, X. Cui, Y. Cui, Z. Bao, *Nano Lett.* **2011**, *11*, 2905.
[12] Z.-S. Wu, D.-W. Wang, W. Ren, J. Zhao, G. Zhou, F. Li, H.-M. Cheng, *Adv. Funct. Mater.* **2010**, *20*, 3595.
[13] W. Sugimoto, H. Iwata, Y. Yasunaga, Y. Murakami, Y. Takasu, *Angew. Chem. Int. Ed.* **2003**, *42*, 4092.
[14] J.-S. Ye, H. F. Cui, X. Liu, T. M. Lim, W.-D. Zhang, F.-S. Sheu, *Small* **2005**, *1*, 560.
[15] K. Fukuda, T. Saida, J. Sato, M. Yonezawa, Y. Takasu, W. Sugimoto, *Inorg. Chem.* **2010**, *49*, 4391.
[16] J. Liu, J. Jiang, C. Cheng, H. Li, J. Zhang, H. Gong, H. J. Fan, *Adv. Mater.* **2011**, *23*, 2076.
[17] X. Lu, D. Zheng, T. Zhai, Z. Liu, Y. Huang, S. Xie, Y. Tong, *Energy Environ. Sci.* **2011**, *4*, 2915.
[18] R. Liu, S. B. Lee, *J. Am. Chem. Soc.* **2008**, *130*, 2942.
[19] W. Yan, T. Ayvazian, J. Kim, Y. Liu, K. C. Donavan, W. Xing, Y. Yang, J. C. Hemminger, R. M. Penner, *ACS Nano* **2011**, *5*, 8275.
[20] X. Lu, T. Zhai, X. Zhang, Y. Shen, L. Yuan, B. Hu, L. Gong, J. Chen, Y. Gao, J. Zhou, Y. Tong, Z. L. Wang, *Adv. Mater.* **2012**, *24*, 938.
[21] Y. Liang, M. G. Schwab, L. Zhi, E. Mugnaioli, U. Kolb, X. Feng, K. Müllen, *J. Am. Chem. Soc.* **2010**, *132*, 15030.
[22] S. K. Meher, G. R. Rao, *J. Phys. Chem. C* **2011**, *115*, 15646.
[23] C. Guan, J. Liu, C. Cheng, H. Li, X. Li, W. Zhou, H. Zhang, H. J. Fan, *Energy Environ. Sci.* **2011**, *4*, 4496.
[24] E. Hosonoa, S. Fujihara, I. Honma, M. Ichihara, H. Zhou, *J. Power Sources* **2006**, *158*, 779.
[25] K.-H. Chang, Y.-F. Lee, C.-C. Hu, C.-I. Chang, C.-L. Liu, Y.-L. Yang, *Chem. Commun.* **2011**, *46*, 7957.
[26] H. Wang, Q. Gao, L. Jiang, *Small* **2011**, *7*, 2454.
[27] H. Wang, H. S. Casalongue, Y. Liang, H. Dai, *J. Am. Chem. Soc.* **2010**, *132*, 7472.
[28] R. Liang, H. Cao, D. Qian, *Chem. Commun.* **2011**, *47*, 10305.
[29] T. Brezesinski, J. Wang, S. H. Tolbert, B. Dunn, *Nat. Mater.* **2010**, *9*, 146.
[30] H. Sun, L. Cao, L. Lu, *Energy Environ. Sci.* **2012**, *5*, 6206.
[31] C.-C. Hu, K.-H. Chang, M.-C. Lin, Y.-T. Wu, *Nano Lett.* **2006**, *6*, 2690.

[32] H. Zhang, G. Cao, Z. Wang, Y. Yang, Z. Shi, Z. Gu, *Nano Lett.* **2008**, *8*, 2664.
[33] C.-C. Hu, C.-Y. Hung, K.-H. Chang, Y.-L. Yang, *J. Power Sources* **2011**, *196*, 847.
[34] P. J. Hall, M. Mirzaeian, S. I. Fletcher, F. B. Sillars, A. J. R. Rennie, G. O. Shitta-Bey, G. Wilson, A. Cruden, R. Carter, *Energy Environ. Sci.* **2010**, *3*, 1238.
[35] M.-Q. Zhao, Q. Zhang, W. Zhang, J.-Q. Huang, Y. Zhang, D. S. Su, F. Wei, *J. Am. Chem. Soc.* **2010**, *132*, 14739.
[36] J. L. Gunjakar, T. W. Kim, H. N. Kim, I. Y. Kim, S.-J. Hwang, *J. Am. Chem. Soc.* **2011**, *133*, 14998.
[37] J. A. Gursky, S. D. Blough, C. Luna, C. Gomez, A. N. Luevano, E. A. Gardner, *J. Am. Chem. Soc.* **2006**, *128*, 8376.
[38] S. Mitchell, I. R. Baxendale, W. Jones, *Green Chem.* **2008**, *10*, 629.
[39] G. Hu, D. O'Hare, *J. Am. Chem. Soc.* **2005**, *127*, 17808.
[40] Y. Wang, W. Yang, S. Zhang, D. G. Evans, X. Duan, *J. Electrochem. Soc.* **2005**, *152*, A2130.
[41] L. Su, X. Zhang, C. Yuan, B. Gao, *J. Electrochem. Soc.* **2008**, *155*, A110.
[42] J. Han, J. Lu, M. Wei, Z. L. Wang, X. Duan, *Chem. Commun.* **2008**, *44*, 5188.
[43] H. Chen, F. Zhang, S. Fu, X. Duan, *Adv. Mater.* **2006**, *18*, 3089.
[44] M. Toupin, T. Brousse, D. Belanger, *Chem. Mater.* **2004**, *16*, 3184.
[45] D. N. Futaba, K. Hata, T. Yamada, T. Hiraoka, Y. Hayamizu, Y. Kakudate, O. Tanaike, H. Hatori, M. Yumura, S. Iijima, *Nat. Mater.* **2006**, *5*, 987.
[46] E. Scavetta, B. Ballarin, M. Gazzano, D. Tonelli, *Electrochim. Acta* **2009**, *54*, 1027.
[47] X. Yang, J. Zhu, L. Qiu, D. Li, *Adv. Mater.* **2011**, *23*, 2833.
[48] C. Liu, Z. Yu, D. Neff, A. Zhamu, B. Z. Jang, *Nano Lett.* **2010**, *10*, 4863.
[49] X. Zhang, W. Shi, J. Zhu, D. J. Kharistal, W. Zhao, B. S. Lalia, H. H. Hng , Q. Yan, *ACS Nano* **2011**, *5*, 2013.

Received: June 15, 2012
Revised: July 25, 2012